

Road Marking Contrast Threshold Revisited

Citation for published version (APA):

Spieringhs, R. M., Smet, K., Heynderickx, I., & Hanselaer, P. (2022). Road Marking Contrast Threshold Revisited. *LEUKOS: The Journal of the Illuminating Engineering Society of North America*, 18(4), 493-512. <https://doi.org/10.1080/15502724.2021.1993893>

Document license:

TAVERNE

DOI:

[10.1080/15502724.2021.1993893](https://doi.org/10.1080/15502724.2021.1993893)

Document status and date:

Published: 01/01/2022

Document Version:

Publisher's PDF, also known as Version of Record (includes final page, issue and volume numbers)

Please check the document version of this publication:

- A submitted manuscript is the version of the article upon submission and before peer-review. There can be important differences between the submitted version and the official published version of record. People interested in the research are advised to contact the author for the final version of the publication, or visit the DOI to the publisher's website.
- The final author version and the galley proof are versions of the publication after peer review.
- The final published version features the final layout of the paper including the volume, issue and page numbers.

[Link to publication](#)

General rights

Copyright and moral rights for the publications made accessible in the public portal are retained by the authors and/or other copyright owners and it is a condition of accessing publications that users recognise and abide by the legal requirements associated with these rights.

- Users may download and print one copy of any publication from the public portal for the purpose of private study or research.
- You may not further distribute the material or use it for any profit-making activity or commercial gain
- You may freely distribute the URL identifying the publication in the public portal.

If the publication is distributed under the terms of Article 25fa of the Dutch Copyright Act, indicated by the "Taverne" license above, please follow below link for the End User Agreement:

www.tue.nl/taverne

Take down policy

If you believe that this document breaches copyright please contact us at:

openaccess@tue.nl

providing details and we will investigate your claim.



LEUKOS

The Journal of the Illuminating Engineering Society

ISSN: (Print) (Online) Journal homepage: <https://www.tandfonline.com/loi/ulks20>


Road Marking Contrast Threshold Revisited

Rik Marco Spieringhs, Kevin Smet, Ingrid Heynderickx & Peter Hanselaer

To cite this article: Rik Marco Spieringhs, Kevin Smet, Ingrid Heynderickx & Peter Hanselaer (2022) Road Marking Contrast Threshold Revisited, LEUKOS, 18:4, 493-512, DOI: [10.1080/15502724.2021.1993893](https://doi.org/10.1080/15502724.2021.1993893)

To link to this article: <https://doi.org/10.1080/15502724.2021.1993893>

 View supplementary material 

 Published online: 16 Dec 2021.

 Submit your article to this journal 




 Article views: 94

 View related articles 

 View Crossmark data 



Road Marking Contrast Threshold Revisited

Rik Marco Spieringhs ^a, Kevin Smet ^a, Ingrid Heynderickx^b, and Peter Hanselaer ^a

^aESAT/Light&Lighting Laboratory, KU Leuven, Ghent, Belgium; ^bIEIS/Human Technology Interaction, TU Eindhoven, Eindhoven, The Netherlands

ABSTRACT

Sufficient contrast between road surface and road markings is key for a safe and comfortable driving experience. This calls for a comprehensive and well established contrast (threshold) model, which ideally results in a single contrast threshold value independent of object angular size or road luminance. The contrast threshold model introduced by Adrian is still commonly used in road lighting. More recently, new contrast metrics that also predict supra-threshold contrast visibility have been proposed, but the corresponding visibility thresholds are not yet known. In the present study, participants are presented a rendering of a highway, including road marking arrows of various size and luminance and were asked to indicate the direction of the arrow. The luminance of the road surface, acting as background for the markings, was varied too. Due to the very low luminance values and the very small differences in luminance, measurement accuracy and calibration issues require special attention. The results show good agreement with Adrian's visibility model ($R^2 = 0.75$) in terms of luminance contrast, background luminance and size. In addition, we used our experimental data to define contrast thresholds for several other existing image based contrast models. Unfortunately, it seems to be impossible to state one unique threshold contrast value independent of object angular size and road luminance.

ARTICLE HISTORY

Received 18 November 2020
Revised 12 October 2021
Accepted 12 October 2021

KEYWORDS

Visibility; road lighting;
target detection; imaging

1. Introduction

Reducing energy consumption while maintaining traffic safety is a main challenge in the design of road lighting. Traffic safety requires a sufficiently high perceived luminance contrast between the road surface and road markings. This luminance contrast is the result of illumination by car headlamps and road lighting in relation to the reflection characteristics of the road surface and the road markings. As LEDs are small-sized light sources, they offer new opportunities in (even asymmetric) beam control using dedicated lenses. In addition, by mainly creating light where it is needed, LEDs offer the opportunity to apply dimming, which contributes to a reduction of energy consumption. An advanced way of reducing energy in road lighting, while maintaining good visibility of objects or signs, is the road lighting concept called “*Probeam*” (Kimura et al. 2019; Sato and Hagio 2014). In this concept, luminaires direct most of their luminous flux forwards, in the direction of view of the driver. One of its objectives is to

illuminate retroreflective road marking arrows at distances beyond the reach of car headlights creating an optimal guide for motorized traffic. To optimize “*Probeam*” in terms of the balance between energy consumption and traffic safety and to define the level of illumination that should be applied in practice, it is essential to understand contrast perception between road markings and the background road surface.

The current study aims to evaluate to what extent the Adrian model (Adrian 1989), known to be accurate in predicting the visibility of targets in uniform backgrounds, can also be used to determine contrast thresholds for the discrimination of the direction of road marking arrows of different size presented on road surfaces, for a set of luminance values attributed to both surfaces. The visual task of determining the direction of a road marking arrow is more complex than just detecting the object itself, and therefore we expect this increase in complexity of the visual task to result in higher

contrast thresholds. More importantly, more recent contrast models, such as a difference of gaussian receptive field model and a pyramidal multilevel model, are explored and the corresponding threshold values have been determined. These models only require a luminance image as input and need no specific information on object angular size, background luminance, or luminance of the target, which would make them more easily applicable in realistic complex scenes. Ideally, each model yields a constant contrast threshold value for detecting the arrow direction, irrespective of the luminance of road and arrow and the size of the arrow.

1.1. State of the art

One of the most prevalent and relevant models within road lighting for determining the visibility of an object is Adrian's contrast threshold model (Brémond 2020). This model is based on predicting the luminance difference threshold needed to see an object and follows both Ricco's and Weber's law (Adrian 1989). This contrast threshold model was extended to road markings by a study of the European commission DG Transport committee described in the COST 331 report (COST 1999).

The relative visual performance (RVP) model, in which the ratio of visual performance (VP) over an optimal VP value is calculated, was introduced by Rea and Ouellette in 1991. The RVP model predicts visual performance rather than only the visibility threshold, and has been applied in commercial and industrial environments (Rea and Ouellette 1991). Although mainly established for indoor lighting, this model has also been used in outdoor lighting (Brémond 2020). However, since our study focuses on finding visibility thresholds and not on supra-threshold visibility performance, the RVP model is not included in our evaluation.

Besides the visual performance and visibility models used for road lighting, there has been an extensive amount of research done on predicting contrast perception in digital images. Image based contrast models can be useful in overcoming the limitations and complications of Adrian's contrast model and Rea's RVP model, such as applications in which heterogeneous backgrounds and targets are involved. Additionally, the image based

contrast models could result in a more applicable visibility metric where the only necessary input is the luminance image. From the many existing contrast models, we here use the most relevant and applicable ones (Simone et al. 2012). They are generally based on two distinguishable concepts of the human visual system: the difference of gaussians (DoG) and the retinal-like subsampling of contrast (Rizzi et al. 2004; Simone et al. 2012; Tadmor and Tolhurst 2000). The first feature was adopted and modified by Tadmor and Tolhurst in 2000, who investigated the usefulness of a DoG based receptive field model for predicting the perception of contrast in natural scenes, as experienced by the retinal ganglion cells and the neurons in the lateral geniculate nucleus (LGN). Later Joulan et al. extended the DoG model by including a multi-scale spatial filter based on parameters determined by the contrast sensitivity function (CSF). The second feature was adopted by Rizzi et al. in 2004 to determine a contrast measure in digital images. In 2012, Simone et al. extended and combined these two features into a weighted level framework model. All these contrast models have in common that no attempt has been made to define threshold values for a discrimination task.

To be able to further optimize new road lighting concepts, the visibility and contrast models mentioned above are evaluated to predict the direction detectability of a road marking arrow. With this application in mind, all models are only evaluated for positive contrasts, in which the arrow is brighter than the road surface background.

2. Adrian's contrast threshold model (1989)

In 1946, Blackwell measured the detectability threshold of a dark spot on a white screen. He indicated that for a decrease in the visual angle and an increase in adaptation brightness, the contrast threshold needed to detect the dark spot increased. Another important observation was that at high brightness and with sufficiently large stimuli, the contrast threshold became linear as a function of adaptation luminance. This relation reflects the Weber-Fechner law of perception.

Later in 1989, Adrian used the data obtained by Blackwell (1946) and combined them with the

contrast threshold data from other studies (Adrian 1969; Aulhorn 1964; Blackwell 1966; Blackwell and Blackwell 1980; Schmidt-Claussen 1969) to determine a model for the visibility of targets, as shown in Equation 1:

$$\Delta L_{threshold} = k \left(\frac{\sqrt{\Phi}}{\alpha} + \sqrt{L} \right)^2 \cdot PF \cdot EF \cdot AF \quad (1)$$

where $\Delta L_{threshold}$ refers to the difference in luminance between target and background at threshold visibility, Φ to the luminous flux function, α to the size of the object in arc minutes, L to the luminance function (i.e., a function related to the background luminance) and k is a constant that is dependent on the experimental conditions. Finally, EF, AF and PF are factors accounting for exposure time, age and contrast polarity, respectively. Adrian's visibility model basically follows a geometric summation based on the Weber-Fechner law (contribution of the luminance function) and Ricco's law (contribution of the luminous flux function) suggested by Berek (1943). For a detailed explanation of these functions and factors we refer to Adrian (1969).

Since the current study concerns positive contrasts, exposure times of 2 seconds and a relatively young group of participants (i.e., students), the contrast polarity, exposure time and age factor are all very close or equal to 1, and as such only a part of Adrian's model is investigated.

3. Image processing contrast models

3.1. Tadmor and Tolhurst (2000)

In 2000, Tadmor and Tolhurst investigated the usefulness of the difference of Gaussian (DoG) receptive field model for predicting the perception of contrast in natural scenes experienced by the retinal ganglion cells and the neurons in the lateral geniculate nucleus (LGN). They assumed that the spatial sensitivity of the center of the receptive field is characterized by a bivariate circular-symmetric Gaussian with a peak amplitude of 1 and a radius r_c . The spatial sensitivity of the surround receptive field is characterized by a second bivariate circular-symmetric Gaussian with a larger radius r_s and a scaled amplitude.

The output of the center receptive field with the midpoint at pixel coordinates x, y is calculated as:

$$R_c(x, y) = \sum_{i=x-3r_c}^{x+3r_c} \sum_{j=y-3r_c}^{y+3r_c} G(i-x, j-y, r_c) L(i, j) \quad (2)$$

where $L(i, j)$ indicates the luminance at the pixel location i, j and $G(i-x, j-y, r)$ represents a bivariate Gaussian centered at x, y and with radius $r = r_c$. The output of the surround receptive field with the midpoint at pixel coordinates x, y is calculated similarly to the center receptive field by Equation 3:

$$R_s(x, y) = \sum_{i=x-3r_s}^{x+3r_s} \sum_{j=y-3r_s}^{y+3r_s} 0.85 \left(\frac{r_c}{r_s} \right)^2 G(i-x, j-y, r_s) L(i, j) \quad (3)$$

The traditional DoG model defines the response of the retinal ganglion cells and the neurons in the LGN as a subtraction of the surround receptive field output from that of the center receptive field:

$$DoG(x, y) = R_c(x, y) - R_s(x, y) \quad (4)$$

Tadmor and Tolhurst suggested some modifications to the traditional DoG model based on the dependency of the gain of the LGN and retinal ganglion cells on the local mean luminance due to the process of light adaptation. The traditional DoG model assumes that the response of a neuron depends solely on the local luminance difference and, therefore, must be normalized by the local mean luminance to account for the process of light adaptation.

This modification of the DoG model by Tadmor and Tolhurst resulted in three hypothetical measures of contrast. The first measure is a normalization based on center adaptation only (C_c):

$$C_c(x, y) = \frac{R_c(x, y) - R_s(x, y)}{R_c(x, y)} \quad (5)$$

The second measure is a normalization based on surround adaptation only (C_s):

$$C_s(x, y) = \frac{R_c(x, y) - R_s(x, y)}{R_s(x, y)} \quad (6)$$

The third measure is a normalization based on an adaptation at both the center and surround receptive field (C_{cs}):

$$C_{cs}(x, y) = \frac{R_c(x, y) - R_s(x, y)}{R_c(x, y) + R_s(x, y)} \quad (7)$$

These measures of contrast result in local contrast values for each pixel p .

3.2. Rizzi, Algeri, Medeghini and Marini (2004)

Another contrast model that was introduced a few years later than the Tadmor and Tolhurst contrast model is the RAMMG model (Rizzi et al. 2004). It refers to the abbreviation of the authors family names. The RAMMG is based on a multilevel analysis using pyramidal under-sampling of a CIELAB lightness image. For each pixel in the lightness image for each of the pyramid layers, a local neighboring contrast value $|P_{p,l} - P_{j,p,l}|$ is calculated. A global contrast estimate (C^{RAMM}) is then provided by taking the average of all the local contrasts over all the different levels, as shown in Equation 8.

$$C^{RAMM} = \frac{1}{N_L} \sum_{l=1}^{N_L} \left(\frac{1}{N_{p,L}} \sum_{p=1}^{N_{p,L}} \left(\sum_{j=1}^8 \frac{|P_{p,l} - P_{j,p,l}|}{8} \right) \right) \quad (8)$$

The number of levels N_L is determined by the pyramidal under-sampling and depends on the resolution of the original image. $N_{p,L}$ marks the number of pixels for a specific pyramid layer and j signifies the eight neighboring pixels of a pixel in the layer.

3.3. Joulan, Hautiere, and Brémond (2011)

In 2011, Joulan et al. proposed a framework to compute the visibility of objects in a luminance image of a road scene based on edge detection (Joulan et al. 2011). The framework exists of two algorithms, one that takes into account the visual adaptation and a second one that uses a set of DoG spatial filters based on coefficients computed from Barten's (1999) contrast sensitivity function (CSF).

The first algorithm applies a gain factor ($1/L_a$) to the input luminance image I_0 where the gain factor is

set to the inverse of the adaptation luminance (L_a), defined as the averaged luminance of I_0 :

$$I_1 = I_0 \frac{1}{L_a} \quad (9)$$

The second algorithm applies a weighted sum of DoG (SDoG) to the image I_1 for a set of filters k :

$$SDoG(I_1) = \sum_k \omega_k G_{\sigma_k^+} - G_{\sigma_k^-}(I_1) \quad (10)$$

where ω_k is the weight of the DoG for filter k , G_{σ} the normalized Gaussian with the standard deviation σ_k^+ for the center and σ_k^- for the surround for filter k . The standard deviation for the center is computed from Barten's CSF and the standard deviation for the surround it is given by $\sigma_k^- = \lambda \sigma_k^+$ with $\lambda = 3$. We refer to Joulan et al. (2011) for more details.

3.4. Simone, Pederson, and Hardeberg (2012)

In 2012, Simone et al. introduced the weighted-level framework (WLF) that includes the DoG model, the pyramidal subsampling with prefiltering, and weights in the recombination of the pyramid layers. Similar to Rizzi et al. the WLF is based on a multilevel analysis using pyramidal subsampling, but it uses an antialiasing filter in addition. For each level of the subsampled RGB image, the local contrast of each pixel is calculated using the Tadmor and Tolhurst DoG model. This results in a local contrast map for each level l , from which the averaged contrast \bar{c} is determined. Subsequently, an overall contrast measure C is calculated for the R, G and B channel separately by a weighted recombination of the average contrast of each level where the weights τ are the variance in local contrast values and N_l the total number of levels. Finally, a global contrast measure $C^{WLF(RSC)}$ is determined by the weighted sum of the overall contrast measure over the three channels where the weights ω are the variance in overall contrast values:

$$C^{WLF(RSC)} = \omega_R C_R^{RSC} + \omega_G C_G^{RSC} + \omega_B C_B^{RSC} \quad (11)$$

where

$$C_R^{RSC} = \frac{1}{N_l} \sum_l^{N_l} \tau_{R,l} \bar{c}_{R,l} \quad (12)$$

$$C_G^{RSC} = \frac{1}{N_l} \sum_l^{N_l} \tau_{G,l} \bar{c}_{G,l} \quad (13)$$

$$C_B^{RSC} = \frac{1}{N_l} \sum_l^{N_l} \tau_{B,l} \bar{c}_{B,l} \quad (14)$$

4. Method

The current study evaluates to what extent existing visibility models can be generalized toward predicting the direction detectability of road marking arrows. Since the existing experimental studies on the visibility of road markings did not focus on the detection of the direction of road marking arrows, a subjective experiment was performed.

4.1. Scenes

For this study, test scenes of a highway were rendered in the physical-based-renderer (PBR) Mitsuba (Jakob 2010), and a 3D model of the scene was created in Blender (Community 2017). The scene was created in different layers by using single Mitsuba renderings of the sky, grass, lamp poles, railing, the road surface, the striped middle road markings, the long left road marking, the long right road marking and the road arrow, as illustrated in Figs. 1 and 2. Since these elements are displayed at relatively large angle from the target in the visual field, it is not expected that the addition of these objects will affect our findings.

After artificially altering the digital counts of each layer, the layers were united into a single image which was then presented to the participants on a calibrated display.

The camera used in Blender to capture the scene and to render in Mitsuba is set at 1.5 m above the road surface and at 1.3 m from the middle striped road marking, aiming 1 degree below the horizontal, simulating the position and viewing direction of a typical (car) driver on a highway (European Committee for Standardization 2015b). The focal

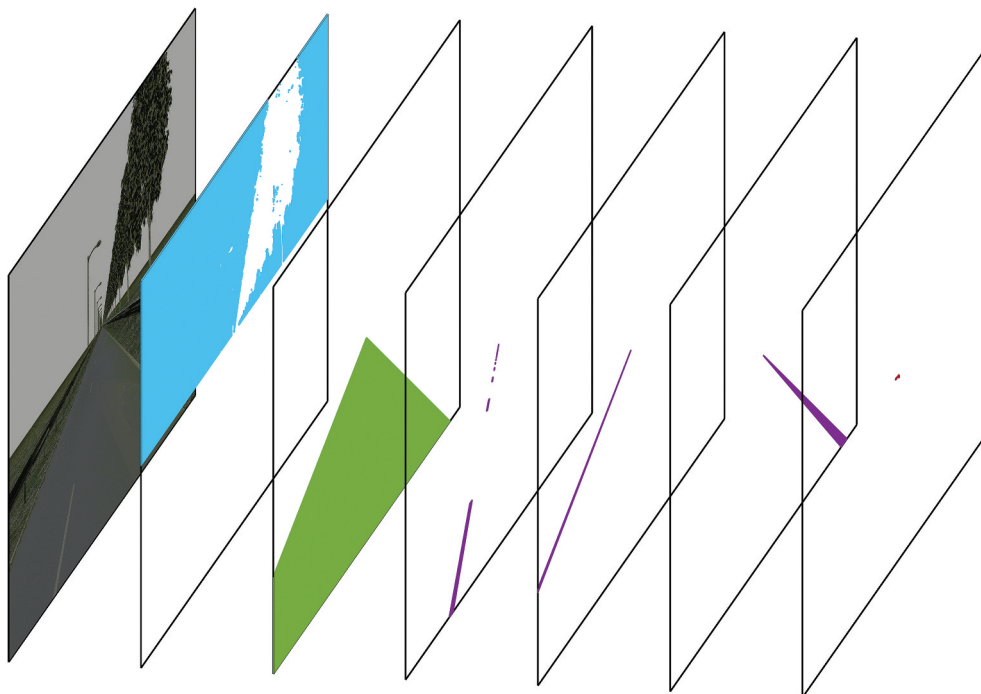


Fig. 1. Example of the separated layers in side view: sky in blue, the road in green, road markings in purple and the road marking arrow in red.



Fig. 2. Example of the separated layers presented in Fig. 1, but now in front view.

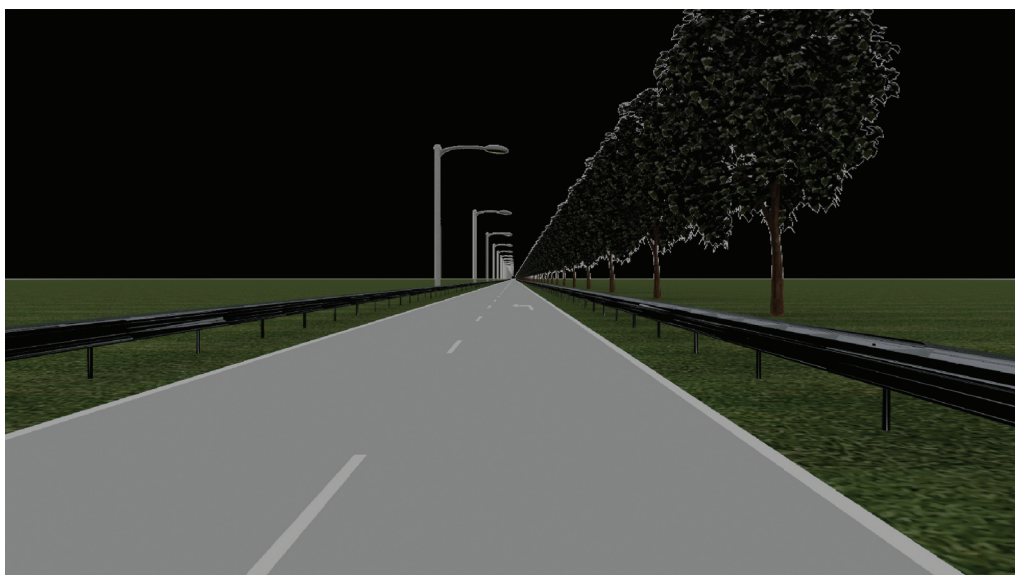


Fig. 3. A representative highway scene rendered by Mitsuba.

length and sensor size of the camera are 16.7 mm and 22.3 mm, respectively. These camera settings are used to simulate the human eye (Mostafawy et al. 1997; Wu et al. 2011).

The road of 7 m wide is split in two lanes of each 3.5 m wide, representing typical dimensions of a Dutch highway (Ministerie van Infrastructuur en Waterstaat 2019). The left and right road markings are 15 cm wide. The middle road markings are 10 cm wide, 3 m long and have a spacing of 9 m (COST 1999). These dimensions correspond to the guidelines for road markings by the

Directorate-General for Public Works and Water Management Rijkswaterstaat (1991). Road markings are always shown in positive contrast to the road surface.

Lamp poles with a height of 18 m are positioned to the left side of the road at 90 m intervals. Trees are placed on the right side of the road at 25 m intervals. To each side of the road, railings and grass planes are added as shown in Fig. 3. The trees, railings, grass plane and lamp posts add complexity to the scene and make the environment more realistic.

4.2. Experimental conditions

For this study, three road luminance values (i.e., 0.25, 0.66 and 0.99 cd/m^2) were selected, representative of typical values found under bad, average and good road lighting conditions (European Committee for Standardization 2015a). For each road luminance value, we determined the required contrast to detect the correct pointing direction of an arrow varying in angular extent (deduced from its distance to a driver position) and luminance. The road arrows were 7.5 m in length and at most 1.05 m in width (Ministerie van Verkeer en Waterstaat, Rijkswaterstaat 1991). The corresponding angular size was calculated in arc minutes based on the plane angle subtended by the length of the road marking in front of the eye (see Fig. 4) at four observer distances (i.e., 40, 60, 80 and 100 m).

To determine a good range of luminance values for the arrows we started with a pilot experiment that followed the exact same protocol as the main experiment (further described below), but with random luminance values for the arrows instead of controlled values. This pilot experiment was executed with 3 observers, and based on its results, we selected five arrow luminance values for each road luminance and each angular size of the arrow. These values are expected to cover



Fig. 4. Image of a road marking arrow with an indication of its length.

Table 1. Five luminance values of the arrow (in cd/m^2) for each combination of road surface luminance (in cd/m^2) and angular length of the arrow (in arcmin).

| Arrow size (') | L_{road} (cd/m^2) | L_{arrow} (cd/m^2) | | | | |
|----------------|---------------------------------------|--|------|------|------|------|
| 20.3 | 0.25 | 0.25 | 0.27 | 0.29 | 0.31 | 0.33 |
| 9.5 | 0.25 | 0.25 | 0.27 | 0.29 | 0.31 | 0.33 |
| 5.5 | 0.25 | 0.27 | 0.29 | 0.31 | 0.33 | 0.35 |
| 3.6 | 0.25 | 0.29 | 0.31 | 0.33 | 0.35 | 0.38 |
| 20.3 | 0.66 | 0.66 | 0.70 | 0.74 | 0.78 | 0.82 |
| 9.5 | 0.66 | 0.66 | 0.70 | 0.74 | 0.78 | 0.82 |
| 5.5 | 0.66 | 0.66 | 0.70 | 0.74 | 0.78 | 0.82 |
| 3.6 | 0.66 | 0.74 | 0.78 | 0.82 | 0.86 | 0.90 |
| 20.3 | 0.99 | 0.99 | 1.04 | 1.09 | 1.14 | 1.19 |
| 9.5 | 0.99 | 0.99 | 1.04 | 1.09 | 1.14 | 1.19 |
| 5.5 | 0.99 | 1.03 | 1.09 | 1.14 | 1.19 | 1.24 |
| 3.6 | 0.99 | 1.09 | 1.14 | 1.19 | 1.24 | 1.29 |



Fig. 5. Picture of the experimental setup, showing the display, chinrest and keyboard.

a visibility range from non-perceptual (50%) to a 100% correct evaluation. Table 1 shows these luminance values, calculated in the CIE 1931 2° color space, because of the small angular extent of our stimuli.

4.3. Experimental setup

The experimental setup consisted of a calibrated 65-inch Samsung QE65Q90 display, a keyboard and a chinrest, as shown in Fig. 5. The display had a resolution of 3840×2160 (4k) pixels and a refresh rate of 120 Hz. The display's absolute full-brightness value was substantially lowered to enable sufficiently high resolution in luminance at the low luminance levels required in the experiment. As a consequence, its maximum luminance (i.e., $R = G = B = 256$) was $33.19 \text{ cd}/\text{m}^2$. The display was positioned perpendicularly to the observer's eyes with its center aligned at the height of the observer's eyes and at a distance of 108 cm. As such, the display covered a vertical and horizontal field of view (FOV) of 42° and 68° , respectively. The experiment took place in a dark room and participants were seated on a chair with their chin

placed on the chinrest. Fixing the eye height and the visual field was needed to match the camera characteristics used to capture the rendered scene in Blender, and hence ensured that distances on the screen matched the physical reality represented in the scene.

4.4. Calibration and measurements

Calibration and characterization of the display were of utmost importance, as we wanted to display small luminance values and luminance differences. To this end, spectral radiance measurements were performed with an air cooled Ocean Optics QE65 Pro spectrometer equipped with a Bentham TEL301 fiber coupled telescope with variable aperture. The integration time of the spectrometer could range from 8 ms up to 15 minutes. Its signal-to-noise ratio was 1000:1 at full signal. The telescope was positioned at a distance of 1.5 m from the display at eye height. Before measuring the stimuli, a dark current measurement was carried out. To convert the spectrometer responses to spectral radiance, two Bentham SRS8 Halogen spectral radiance standards were used. For measuring the low luminance values of our experiment, an aperture size of 3.5 mm was required, but this resulted in saturation when targeting the radiance standard. A second radiance standard, equipped with a neutral density filter with optical density 0.9, was calibrated with respect to the primary radiance standard using a smaller aperture (i.e., 1.17 mm).

To bridge the dynamic range between the calibration standard and our low-luminance stimuli, linearity of the detector response with integration time was crucial. This was checked by measuring the response of a 150×150 pixels stimulus located at the middle of the display, driven with an 8-bits signal of $R = G = B = 150$. The size of this stimulus was slightly larger than the field of view of the spectrometer. The position of the stimulus was identical to the position of the road marking arrows during our experiment. The stimulus was measured at 16 integration times, varying between 0.027 and 58 seconds. The dark current response was also measured and subtracted.

The dark corrected spectrometer response for each peak wavelength as a function of integration

time confirms the spectrometer's linearity with integration time.

Finally, we checked the stability of the display over time. To this end, a 150×150 pixel square with an 8-bits signal of $R = G = B = 150$ was measured 29 times over the course of several days. The first 21 measurements were taken within the first 1.5 hours and resulted in a mean luminance of 1.55 cd/m^2 and a standard deviation of 0.002 cd/m^2 . Three measurements were taken the day after and, even without recalibration, yielded a mean luminance of 1.55 cd/m^2 and a standard deviation of 0.002 cd/m^2 . Four other measurements were taken five days later resulting in a mean luminance of 1.54 cd/m^2 and a standard deviation of 0.0007 cd/m^2 . These results show the high stability of the display and the accuracy of the measuring process.

The whole calibration and measurement procedure resulted in an accurate look-up table relating RGB-values to actual luminance values.

4.5. Design and procedure

In the experiment, participants had to judge the direction (i.e., left or right) of a road marking arrow on a road surface using the method of constant stimuli (Gescheider 1997). We used a full-factorial semi-between subject design with the luminance of the road surface (i.e., 3 levels: 0.25, 0.66 and 0.99 cd/m^2), the luminance of the road marking arrow (i.e., 5 levels depending on the road surface luminance) and the arrow's angular size (i.e., 4 levels: 20.3, 9.5, 5.5 and 3.6 arcmin) as independent semi-between subject variables and the luminance difference thresholds (as defined below) as the dependent variable. In total, each participant had to judge 1 road surface luminance value, 5 luminance values of the road arrow, 4 angular sizes of the arrow and 2 directions (arrow pointing left or right), with each condition repeated ten times, which resulted in 400 stimuli (i.e., $5 \times 4 \times 2 \times 10$). Participants were split into three groups, one for each value of the road surface luminance.

Before starting the experiment, participants that were not familiar with its procedure received an introduction, in which possible unclarities were resolved and a few trials were performed. After

these trials, the participants were requested to adapt to a gray image (subtending 3840×2160 pixels at $R = G = B = 119$, which corresponded to 0.31 cd/m^2) for two minutes in a dark room such that the impact of previous adaptation to any reference was minimized. After this adaptation period, the experiment started with a full gray image shown for 3 seconds. Afterward, we displayed one of our stimuli for 2 seconds, followed by again the full gray adaptation image for 3 seconds. Participants were instructed to indicate whether the arrow on the road was pointing to the left or right, by pressing the corresponding arrow key on the keyboard. Responses could only be given while the stimulus was on the display screen, so a maximum of 2 seconds response time was used. If a participant correctly identified the direction of an arrow a response of 1 was recorded, and when a participant incorrectly identified the direction of an arrow a response of 0 was recorded. When participants did not observe any arrow, they could abstain from responding. When a participant did not give a response within the time of exposure (i.e., 2 s) a value of 0.5 was recorded (i.e., assuming to be the average response of having to guess between two equal options). All stimuli were presented in random order. The experiment took about 45 minutes to finish.

4.6. Participants

Participants were recruited among the members of the authors' lab and interested students. In total, 18 participants conducted the experiment, i.e., 6 per road luminance condition. Of these 18 participants 6 were female and 12 male. The participants were aged from 18 to 35 years old, with an average age of 26.9 years ($SD = 3.1$).

5. Results

5.1. Analysis of the experiment

Each scene has been evaluated 10 times by each observer. In the analysis, proportion of correct responses for each participant, at each road surface luminance and angular size of the arrow (i.e., $3 \times 4 = 12$ combinations) were plotted against the

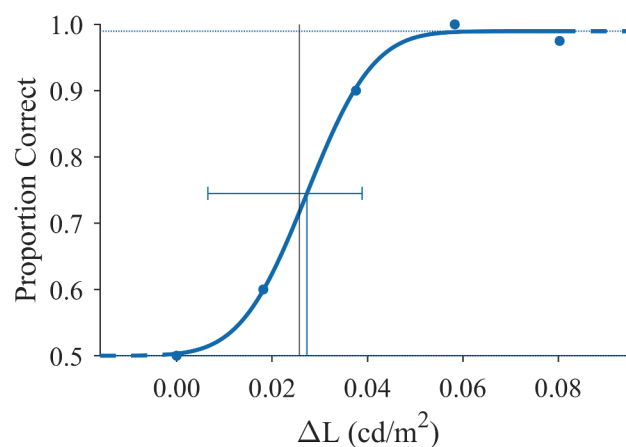


Fig. 6. The psychometric curve (solid blue line) for participant 1 measured for a road surface luminance of 0.25 cd/m^2 and an arrow's angular size of 9.5 min as a function of the luminance difference between arrow and road surface. The threshold is determined from the 0.75 proportion correct, and the corresponding confidence interval is indicated by the horizontal blue line. The corresponding threshold estimated by Adrian (including age) is indicated with the vertical black line.

difference in luminance of the road marking arrow with the road surface. A psychometric curve was fitted through these plots per participant, road surface luminance and angular size of the arrow. The luminance difference threshold was defined as the 0.75 proportion correct.

Initially, we considered the Wichmann and Hill method (2001a) for fitting the psychometric curves, using the Monte Carlo simulation of bootstrap. However, previous research indicated that the confidence intervals obtained by bootstrapping may be too small (Fründ et al. 2011; Hill 2002; Kuss et al. 2005) in case of small data sets. Therefore, considering the small data set of our study as well, more credible intervals were determined with Bayesian statistics (Schütt et al. 2016; Wichmann and Hill 2001b). In this approach, the intervals were calculated based on a standard prior, cumulative Gaussian distribution and a fixed lower asymptote at 0.5 with the *psignifit* (v.4) software that used the formulae provided by Schütt et al. (2016). Figure 6 shows as an example the psychometric function of participant 1 for a road surface luminance of 0.25 cd/m^2 and an angular size of the arrow of 9.5 arcmin .

For all participants and all 12 combinations of road surface luminance and angular size of the arrow, the psychometric curve was successfully

fitted (with an average R^2 of 0.91 and R^2 values ranging between 0.25 and 1.00¹), except for participant 10 at a road surface luminance of 0.25 cd/m² and an arrow angular size of 3.6 arcmin, in which condition the data was overly dispersed (R^2 of -0.88). Nevertheless, even for this participant a best threshold estimate was provided by the *psignifit* (v.4) software. We also investigated “pooling” the data over the six participants and then fit a normal cumulative distribution to the combined dataset, however, found the results to be similar.

For determining the inter-observer variability, the standard residual sum of squares (STRESS) was calculated as provided by Garcia et al. (2007), for each road surface luminance separately (i.e., 6 observers), as shown in Equations 15 and 16:

$$\text{STRESS} = \frac{1}{6} \sum_{i=1}^6 \left(\frac{\sum_{j=1}^4 (E_{ij} - fV_j)^2}{\sum_{j=1}^4 (fV_j)^2} \right)^{1/2} \quad (15)$$

with

$$f = \frac{\sum_{j=1}^4 (E_{ij})^2}{\sum_{j=1}^4 E_{ij}V_j} \quad (16)$$

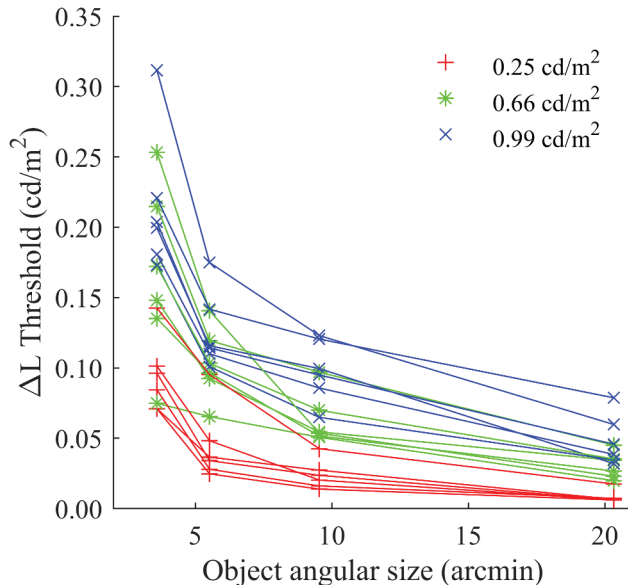


Fig. 7. The luminance difference threshold for each of the 6 observers plotted against the arrow size (i.e., 20.3, 9.5, 5.5, 3.6 arcmin) for each road surface luminance (i.e., 0.25, 0.66 and 0.99 cd/m²).

and E_{ij} indicates the luminance difference threshold of observer i for the angular size of the road arrow j and V_j indicates the luminance difference threshold averaged over all (six) observers for the angular size of the road arrow j . The resulting STRESS values were converted to percentages by multiplying them by 100. The STRESS percentages for the 0.25, 0.66 and 0.99 cd/m² road surface luminance were 11, 10 and 5%, respectively. As suggested in the multidimensional scaling literature these STRESS percentages would be considered around fair (10%) to good (5%) (Garcia et al. 2007; Kruskal 1964).

Figure 7 shows the luminance difference thresholds obtained from the psychometric fits. It clearly shows that the luminance difference threshold decreases with increasing arrow size, and decreasing road luminance (or background luminance).

To confirm the statistical significance of the decrease in luminance difference threshold with increased angular size of the arrow and decreased background luminance, we performed a mixed repeated-measures factorial ANOVA with the road surface luminance and arrow angular size as independent factors (including also their interaction) and with the measured luminance difference threshold as dependent factor. The arrow angular size was taken as a within-subject independent variable, while the road surface luminance was included as a between-subject factor. Prior to further analysis, the assumptions of homogeneity of variance and sphericity were checked. For the within-subject variable, the sphericity hypothesis according to the Mauchly's test across the four angular sizes of the arrow was rejected ($p < .05$); therefore a Greenhouse-Geisser correction was used. The Levene's test of equality of error variances was rejected only for the arrow angular size of 20.3 arcmin ($p = .026$). Since this implies that variance was similar for all other angular sizes and road surface luminance values, still a mixed repeated-measures factorial ANOVA was used. This analysis revealed a statistically significant main effect for the angular size of the arrow ($F_{18.1,1.2} = 123.96$; $p < .001$; $\eta^2 = .89$) and for the road surface luminance ($F_{15,2} = 17.24$; $p < .001$; $\eta^2 = .70$). Furthermore, it revealed a significant interaction

¹ R^2 throughout the paper refers to the Coefficient of Determination.

between arrow angular size and road surface luminance ($F_{18,1,2,4} = 3.98$; $p < .05$; $\eta^2 = .35$). These effects are not surprising, as similar findings were reported before in Cao (2004) and Mayeur et al. (2010).

5.2. Applicability of the Adrian model

To compare our experimentally measured luminance difference threshold values with the values predicted by the visibility model of Adrian, we calculated their mean value over all observers (and the respective 95% confidence interval) per road surface luminance and arrow angular size. The resulting mean luminance difference thresholds as a function of road surface luminance for the different values of the angular size of the arrow, and as a function of angular size of the arrow for the different values of the road surface luminance were fitted with Adrian's model using Equation 1. The resulting fits are shown in Figs. 8 and 9, respectively. In both figures, the solid lines indicate the predicted visibility by Adrian's model, while the experimental data are shown by the crosses and their 95% confidence interval.

Figure 10 presents the overall correspondence between our experimental data and Adrian's model

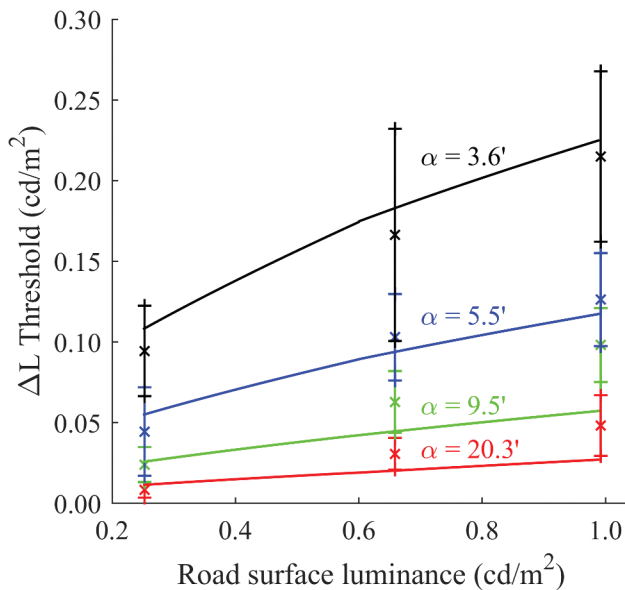


Fig. 8. The measured luminance difference threshold plotted as a function of the road surface luminance for different values of the angular size of the arrow (separated by color). The means of the measured thresholds per condition are indicated by crosses and at each cross the corresponding 95% confidence interval is shown. Solid lines indicate the prediction by Adrian's model.

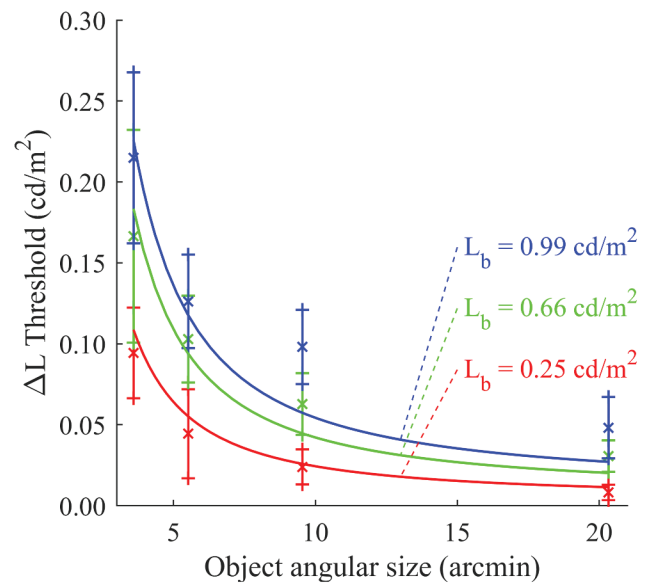


Fig. 9. The measured luminance difference threshold plotted as a function of the arrow angular size for different values of the road surface luminance (separated by color). The means of the measured thresholds per condition are indicated by crosses and at each cross the corresponding 95% confidence interval is shown. Solid lines indicate the prediction by Adrian's model.

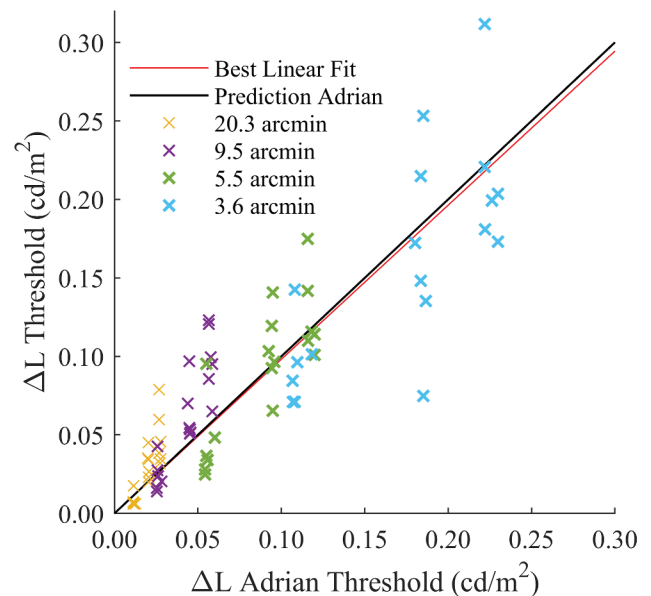


Fig. 10. Our measured data plotted against the thresholds predicted by the visibility model of Adrian (black line). Crosses indicate the observed threshold for each participant and condition. The red line gives the best fit for an optimized model parameter k of 2.55.

in a scatter plot. The solid black line indicates perfect correspondence for a visibility level equal to 1 following the standard Adrian's model for detection thresholds. Two goodness-of-fit values are determined: one

with the model parameter k (see Equation 1) taken as 2.6 (i.e., the recommended value for a forced-choice method (Adrian 1989)), and one using a best fit after optimizing the model parameter k . They result in R^2 values of 0.75 and 0.75, respectively. In addition, Fig. 10 also shows that the “best fit” line is very close to Adrian’s model, indicating that the thresholds needed for discriminating the direction of an arrow can be estimated with Adrian’s detection threshold model without taking into account the anticipated higher thresholds because of the higher complexity of the visual task.

5.3. Thresholds for the Tadmor & Tolhurst model

For each scene presented to the observers, we calculated the Difference of Gaussian (DoG) value (as proposed by Tadmor and Tolhurst) per pixel in a frame of 150×150 pixels around the road marking arrow. We chose to use one fixed frame to encompass all road marking arrows, where the largest arrow (i.e., 20.3 arcmin) covered 2.3% of the frame, whereas the smallest arrow (i.e., 3.6 arcmin) covered 0.4% of the frame. To calculate the DoG value per pixel, we first converted the RGB-image within the frame to a luminance image using using the look-up table (mentioned in section 4.4 Calibration and measurements). We then applied the DoG model (Equations 2, 3 and 4) with some modifications.

The first modification is that we wanted to use a global DoG value per scene C_{DoG} , and therefore, summed all local DoG-values over the N_p (i.e., 150×150) pixels of the image (Donners et al. 2015; Scheir et al. 2018):

$$C_{DoG} = \sum_{p=1}^{N_p} |DoG(x, y)| \quad (17)$$

To do so, we replaced the DoG values by their absolute values in order to avoid compensation when adding positive and negative DoG pixel values (Donners et al. 2015; Scheir et al. 2018).

Second, instead of using the 0.85 weighting factor in the calculation of the surround receptive field (Equation 3), we chose a center/surround weighting factor of 1, which ensured that a region of uniform luminance extending from the edge of the surround receptive field did not contribute to C_{DoG} . As

a consequence, the amount of background pixels included on the final C_{DoG} value was much lower. Finally, although theoretically the DoG value of a pixel for which the center and surround is completely covering a uniform luminance region is meant to be zero, the discrete integral approximation as proposed by Tadmor and Tolhurst resulted in a small value of 0.00067. Although very small, when multiplied by the whole frame (of 150×150 pixels), this might become such a large value that it masked the contribution of the fewer pixels signaling real contrast. To obtain an absolute zero DoG value for a uniform center and surround, the discrete integral values of the two bivariate Gaussians were rounded to five decimals and slightly adjusted to the values shown in the supplemental material.

Finally, the center radius r_c was set at 1 pixel and the surround radius r_s at 2 pixels, resulting in a center/surround ratio of 1:2. As the images were projected on a screen with a field of view of 42° vertically and 68° horizontally, each pixel represented 0.89 arcmin horizontally and 1.17 min vertically. As such, the center radius r_c of 1 pixel was in line with the angular resolution of the eye of 0.7 to 0.8 arcmin (Clark 1990; Curcio et al. 1990) at the fovea. The center to surround ratio of the receptive field radii corresponded to the ratio reported by

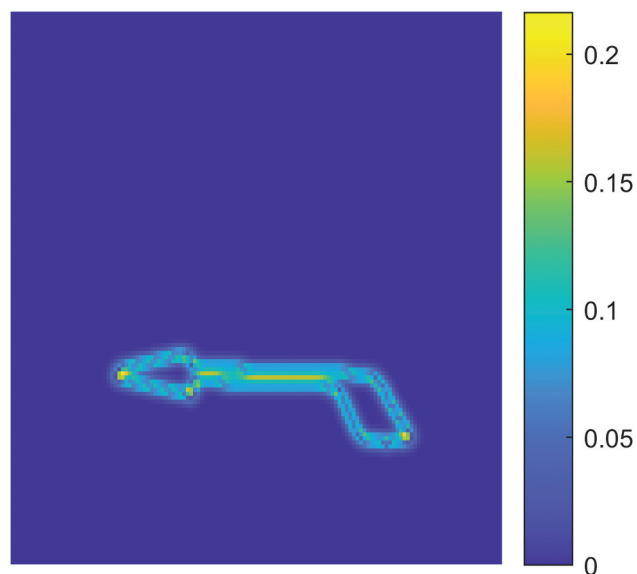


Fig. 11. DoG-filtered image of the 150×150 pixels of a road marking image for a road surface luminance of 0.99 cd/m^2 , road marking luminance of 1.19 cd/m^2 and an arrow’s angular size of 20.3 arcmin. The color bar at the right indicates the DoG values that correspond to the colors.

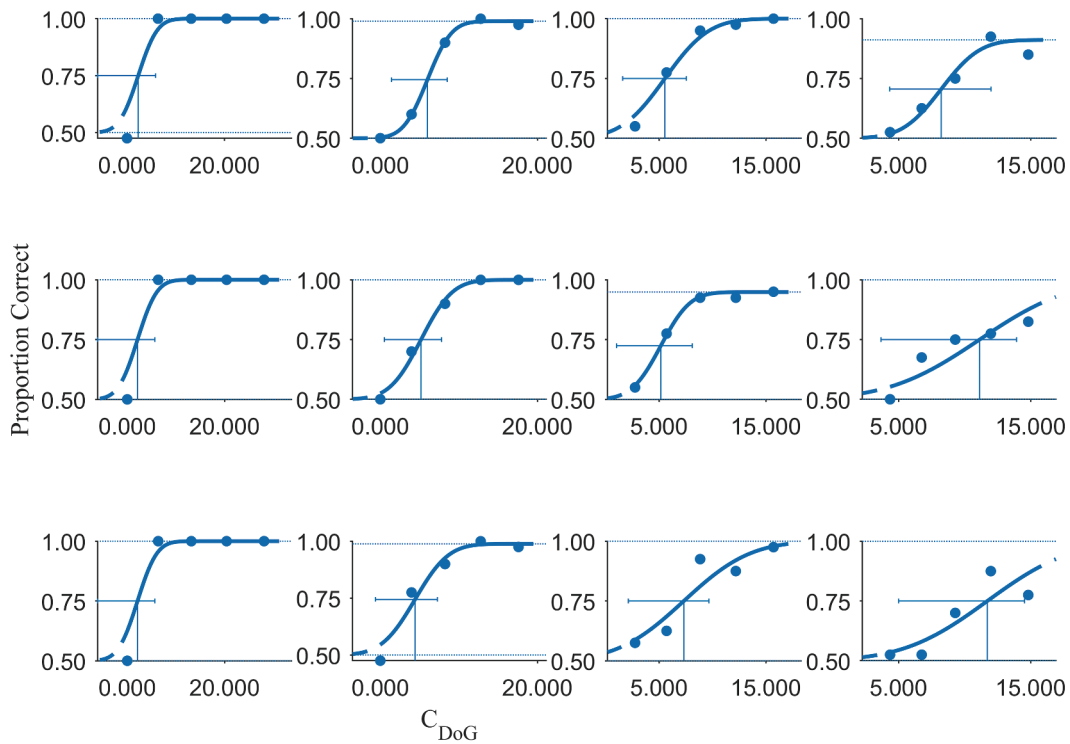


Fig. 12. The psychometric curves fitting the proportion correct responses as a function of C_{DoG} values for participant 1, 2 and 3 (from top to bottom, respectively). The psychometric curves were plotted for each angular size of the arrow: i.e., 20.3, 9.5, 5.5 and 3.6 arcmin (from left to right, respectively). All plots refer to a road surface luminance of 0.25 cd/m^2 .

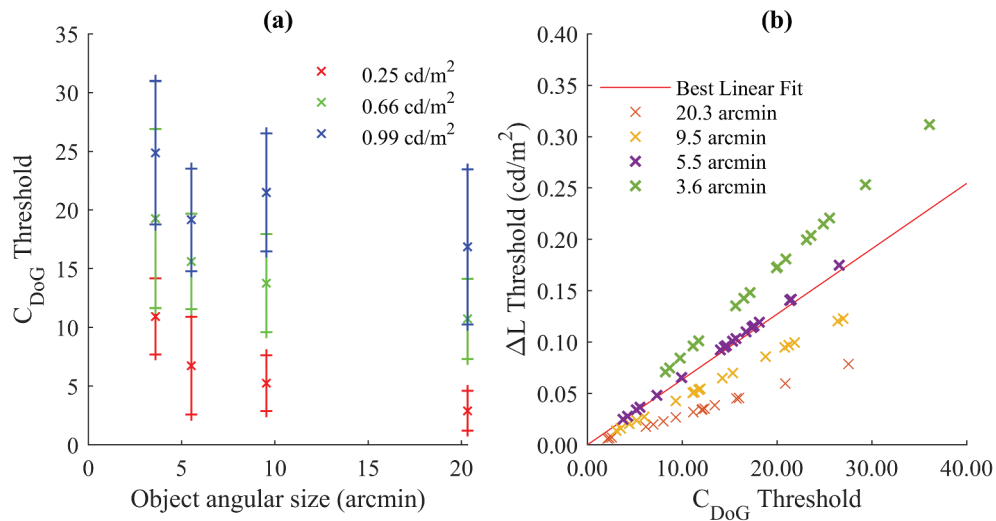


Fig. 13. (a) The averaged C_{DoG} thresholds (indicated by the crosses) and their 95% confidence interval plotted against the angular size of the arrow for each road surface luminance (i.e., 0.25, 0.66 and 0.99 cd/m^2). (b) Our measured data plotted against the C_{DoG} thresholds. Crosses indicate the observed threshold for each participant and condition. The red line gives the best fit ($R^2 = 0.72$).

Simone et al. (2012). An example of a DoG-filtered image is given in Fig. 11.

We then plotted psychometric curves (in the same way as explained before), but now using the calculated C_{DoG} values instead of ΔL values at the ordinate. Figure 12 illustrates these psychometric

curves for participant 1, 2 and 3, indicating the proportion correct responses for the four different angular sizes of the arrow, measured for a road surface luminance of 0.25 cd/m^2 . All psychometric curves result in an average R^2 of 0.91 and R^2 -values ranging between 0.25 and 1.00 indicating a good fit

to the data, except for participant 10 at a road surface luminance of 0.25 cd/m^2 and angular size of 3.6 min of the arrow. As explained before, the latter data were overly dispersed (R^2 of -0.88).

The mean C_{DoG} thresholds (corresponding to the C_{DoG} -value at 0.75 proportion correct, averaged over all 6 participants per road surface luminance) are plotted in Fig. 13(a) together with their 95% confidence interval (calculated using Bayesian statistics), similar as in Fig. 9. Fig. 13(b) presents the overall linearity between our experimental data and the C_{DoG} thresholds in a scatter plot, similar as in Fig. 10. Overall, threshold values decrease with increasing angular size and decreasing road luminance, in analogy with the luminance difference thresholds. If, the C_{DoG} model would perfectly correlate with the discrimination of an arrow's direction, one unique C_{DoG} threshold value would emerge, irrespective of background luminance and angular size of the arrow.

Unfortunately, this is not the case. The average C_{DoG} threshold value at 0.66 cd/m^2 background luminance varies over 44% between the highest and lowest value across all angular sizes of the arrow. The average C_{DoG} threshold values at 0.66 cd/m^2 background luminance vary over about 44% between the highest and lowest value across all angular sizes of the arrow. The variation in threshold values at 10 arcmin angular size

across the various levels of the road surface luminance numbers 76%. Note that the C_{DoG} model indeed does not include a global adaptation factor.

In addition to determining the C_{DoG} thresholds also, similarly, the thresholds for the normalized contrast estimates (C_c , C_s , and C_{cs}) were determined based on Equations 5–7. For the contrast estimates C_c , C_s , and C_{cs} , all psychometric curves resulted in an average R^2 of 0.91 and R^2 -values ranging between 0.25 and 1.00 indicating a good fit to the data, except for participant 10 at a road surface luminance of 0.25 cd/m^2 and angular size of 3.6 min of the arrow. The mean C_c , C_s , and C_{cs} threshold values (again, corresponding to the 0.75 proportion correct, averaged over the six participants per road surface luminance) are plotted in Fig. 14 together with their 95% confidence interval. Overall, threshold values decrease with increasing angular size. The average C_c , C_s , and C_{cs} threshold values at 0.66 cd/m^2 background luminance vary over about 44% between the highest and lowest value across all angular sizes of the arrow. The variation in threshold values at 10 arcmin angular size across the various levels of the road surface luminance is about 0.051%. The overall linearity between our experimental data and the C_c , C_s , and C_{cs} thresholds is presented in separate scatter plots in Fig. 15.

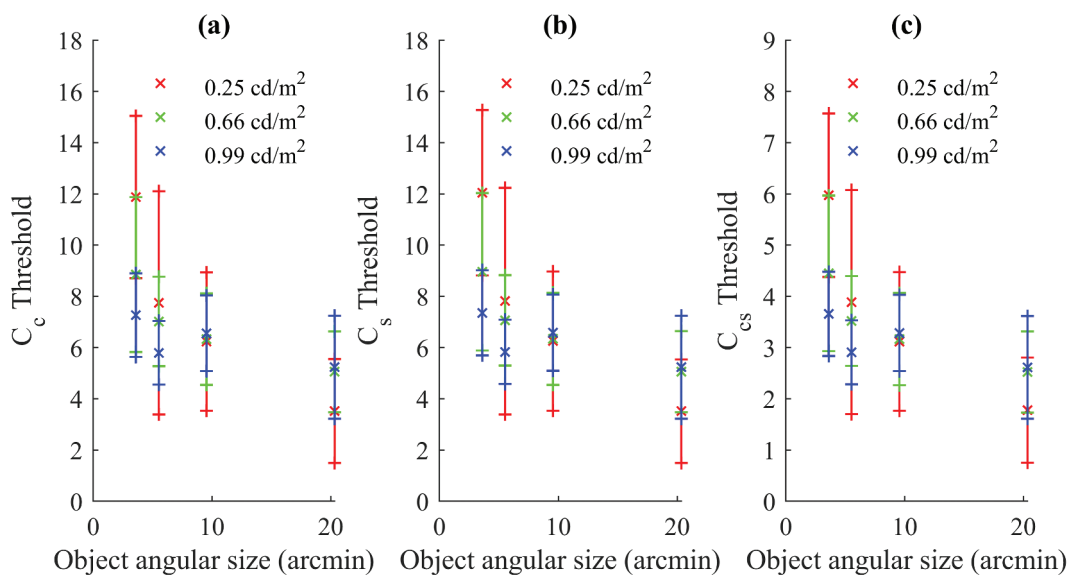


Fig. 14. The averaged C_c (a), C_s (b), and C_{cs} (c) thresholds (indicated by the crosses) and their 95% confidence interval plotted against the angular size of the arrow for each road surface luminance (i.e., 0.25 , 0.66 and 0.99 cd/m^2).

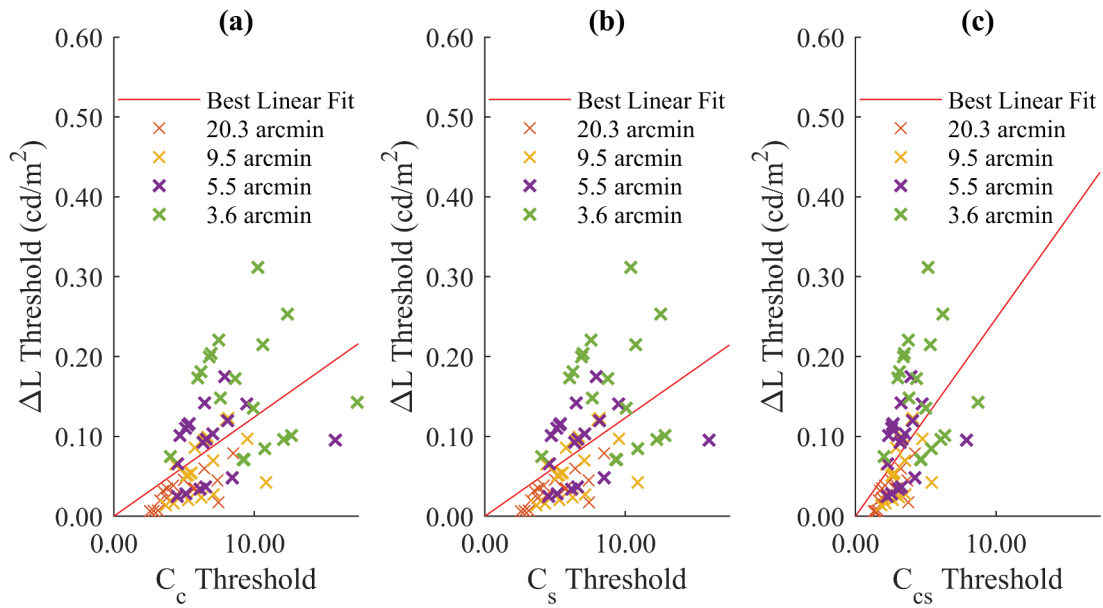


Fig. 15. Our measured data plotted against the C_c (a), C_s (b), and C_{cs} (c) thresholds. Crosses indicate the observed threshold for each participant and condition. The red line gives the best fit ($R^2 = 0.28$ (a), 0.28 (b), 0.28 (c)).

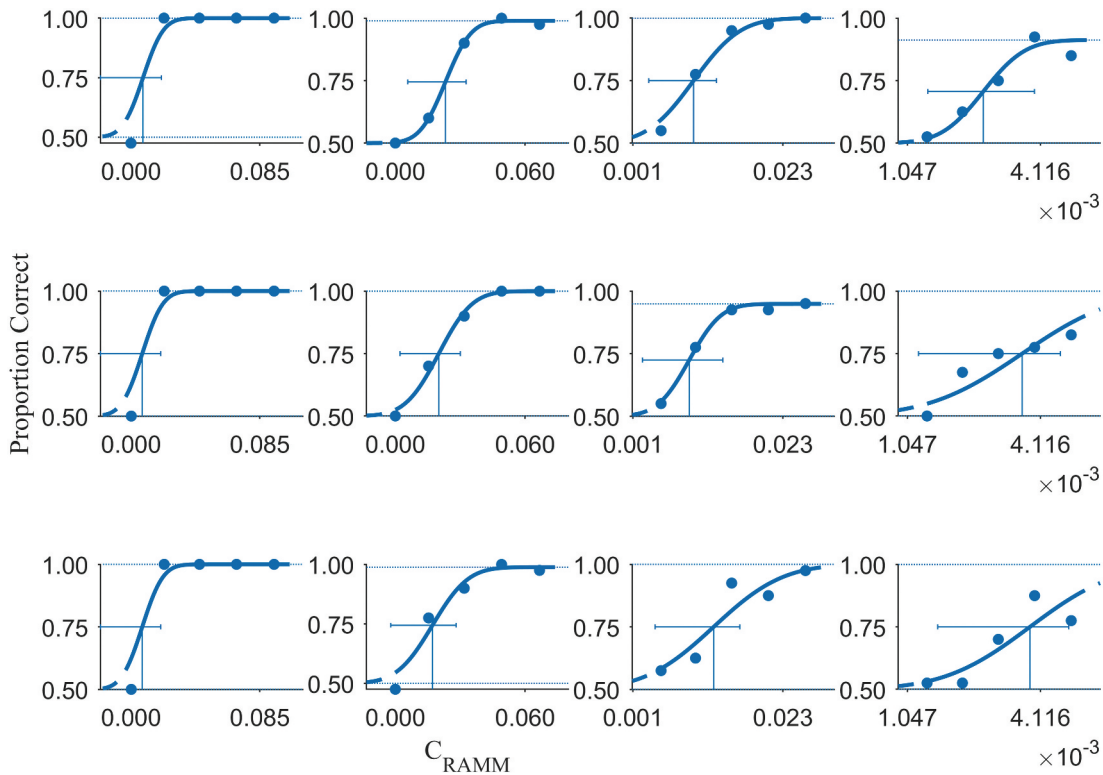


Fig. 16. Psychometric curves fitted through the proportion correct responses as a function of the C_{RAMM} values. The plotting arrangement is similar as in Fig. 12.

5.4. Thresholds for the Rizzi et al. model

In addition to determining the thresholds with the C_{DoG} model, we determined the C_{RAMM} threshold

contrast values for each angular size, road surface luminance and road marking luminance. Again, the RGB image of 150×150 pixels around the

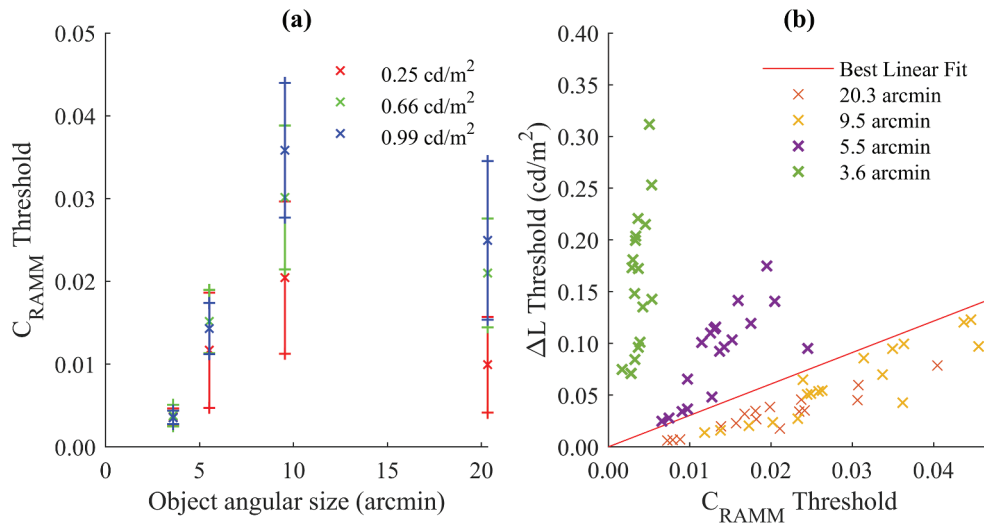


Fig. 17. (a) The averaged C_{RAMM} threshold values (indicated by the crosses) and their 95% confidence interval plotted against the angular size of the arrow for each road surface luminance (i.e., 0.25, 0.66 and 0.99 cd/m^2). (b) Our measured data plotted against the C_{RAMM} thresholds. Crosses indicate the observed threshold for each participant and condition. The red line gives the best fit ($R^2 = -0.85$).

road marking arrow was converted into a luminance image, and subsequently used to calculate the C_{RAMM} values according to Equation 8. Also these C_{RAMM} values were compared to the proportion correct, and these data were used to fit psychometric curves, as illustrated in Fig. 16. Similarly, as with the other contrast measures, the psychometric curves resulted in an average R^2 of 0.91 with R^2 values ranging between 0.25 and 1.00, except for participant 10 at a road surface luminance of 0.25 cd/m^2 and an angular size of 3.6 arcmin of the arrow.

The averaged C_{RAMM} threshold values (again, corresponding to 0.75 proportion correct, averaged over the six participants per road surface luminance) are plotted in Fig. 17(a) together with their 95% confidence interval, similar as in Figs. 9, 13(a) and 14. Figure 17(b) presents the overall linearity between our experimental data and the C_{RAMM} thresholds in a scatter plot, similar as in Figs. 10, 13(b), and 15. The average C_{RAMM} threshold value at 0.66 cd/m^2 road surface luminance varies over 87% between the highest and lowest value across the various angular sizes. The variation in threshold values at 10 arcmin angular size across the various levels of the road surface luminance numbers 34%.

5.5. Joulan et al. model

To compare our experimentally measured arrow-direction detection thresholds to the Joulan et al. visibility model, we transferred all stimuli (i.e., for each angular size, road surface luminance and road marking luminance) into SDoG-values using Equation 10, but with a similar modification as what we used in the Tadmor and Tolhurst model, i.e., that we summed all C_{SDoG} -values over the N_p (i.e., 150×150) pixels of the image, resulting in:

$$C_{SDoG} = \sum_{p=1}^{N_p} SDoG(x, y) \quad (18)$$

Subsequently, the proportion correct arrow-direction detections were plotted against the resulting C_{SDoG} -values, and fitted to a psychometric curve. Overall, also the C_{SDoG} -values yielded good fits of the psychometric function to the fraction correct answers with a goodness of fit very comparable to the other visibility measures we considered so far (i.e., an average R^2 of 0.91 and R^2 -values ranging between 0.25 and 1.00). The mean C_{SDoG} -threshold values (again, corresponding to 0.75 proportion correct, averaged over the six participants per road surface luminance) are plotted in Fig. 18(a) together

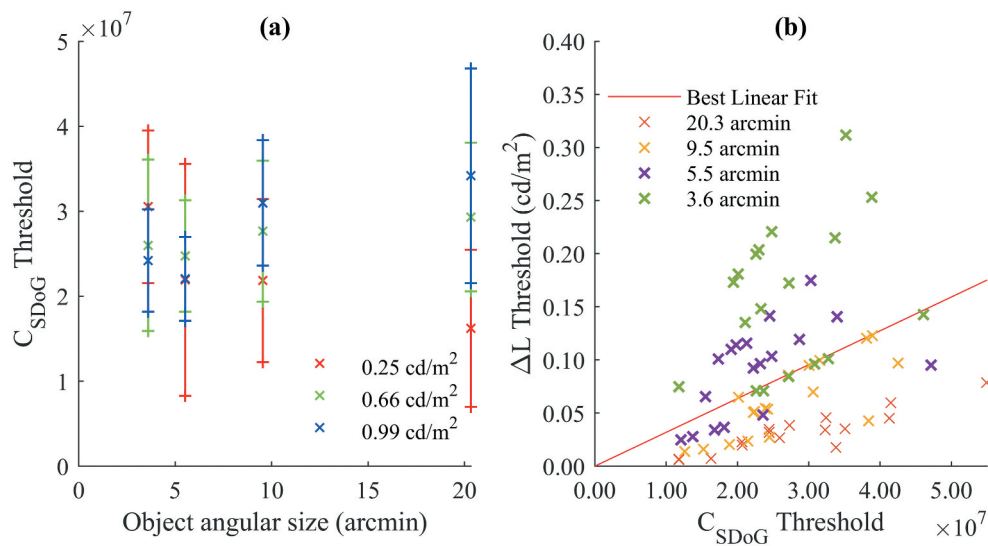


Fig. 18. (a) The averaged C_{SDoG} threshold values (indicated by the crosses) and their 95% confidence interval plotted against the angular size of the arrow for each road surface luminance (i.e., 0.25, 0.66 and 0.99 cd/m^2). (b) Our measured data plotted against the C_{SDoG} thresholds. Crosses indicate the observed threshold for each participant and condition. The red line gives the best fit ($R^2 = 0.092$).

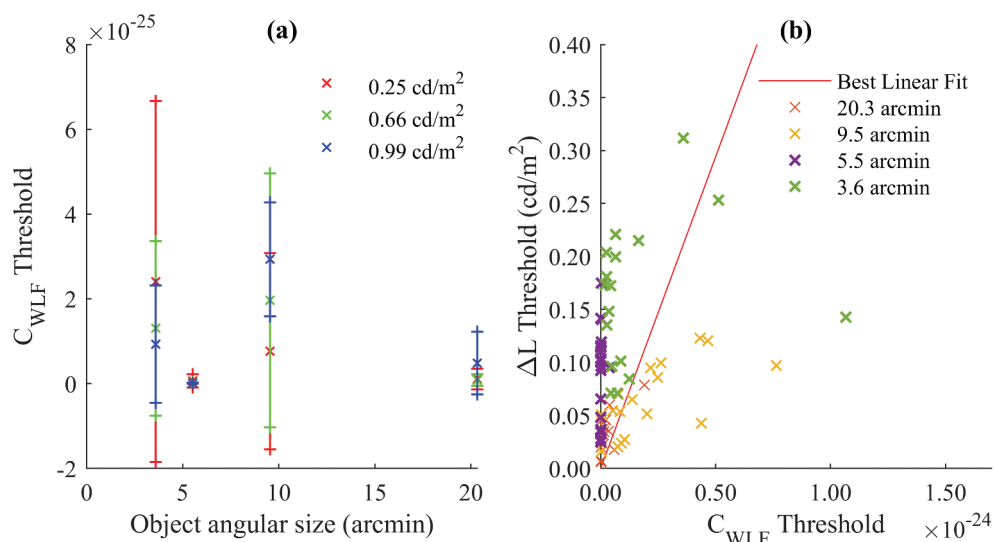


Fig. 19. (a) The averaged C_{WLF} threshold values (indicated by the crosses) and their 95% confidence interval plotted against the angular size of the arrow for each road surface luminance (i.e., 0.25, 0.66 and 0.99 cd/m^2). (b) Our measured data plotted against the C_{WLF} thresholds. Crosses indicate the observed threshold for each participant and condition. The red line gives the best fit ($R^2 = -12.00$).

with their 95% confidence interval. When compared to the average contrast threshold values of other contrast models, the average C_{SDoG} threshold values show more consistency across different angular sizes of the arrow for a given road surface luminance. The average C_{SDoG} threshold value at 0.66 cd/m^2 road surface luminance varies over 16% between the highest and lowest value across the various angular sizes. The variation in threshold values at 10 arcmin angular size across the various levels of the road surface

luminance numbers 30%. The overall linearity between our experimental data and the C_{SDoG} thresholds is illustrated in a scatter plot in Fig. 18(b).

5.6. Simone et al. model

The Simone et al. model is the final one that we evaluated for predicting our experimental data. Also in this case we calculated for each angular size, road surface luminance and road marking luminance the

corresponding C_{WLF} -value, using Equations 11–14 on the RGB images with a size of 150×150 pixels. The proportion correct responses measured in the experiment were then plotted as a function of the resulting C_{WLF} -values, and these data were used to fit psychometric curves. The resulting psychometric curves fitted the data somewhat less well than for the earlier visibility models we evaluated, since the average R^2 is reduced to 0.75 (from around 0.9). From the fits, we determined the mean C_{WLF} -threshold values (again, corresponding to 0.75 proportion correct, averaged over the six participants per road surface luminance), and plotted them in Fig. 19(a) as a function of the angular size of the arrow, together with their 95% confidence interval. When compared to the average contrast threshold values of other contrast models, the average C_{WLF} threshold values show less consistency across different angular size road surface luminance (99% variation over angular size at 0.66 cd/m^2 road surface luminance and 74% variation over road surface luminance at 10 arcmin angular size). The overall linearity between our experimental data and the C_{WLF} thresholds is shown in a scatter plot in Fig. 19(b).

6. Discussion

Our experimentally measured thresholds between a road marking luminance and the road surface luminance corresponded well ($R^2 > 0.7$) with the luminance difference thresholds predicted by the visibility model of Adrian. Our participants had to indicate the pointing direction of a road arrow, which is a considerably different paradigm from the one used before by Blackwell (1946), where participants had to indicate the presence of a stimulus. In that sense, it is a surprising result that the visibility model of Adrian predicts our experimental results so well; it shows that the model is more broadly applicable than where it originally was intended for. Although the results in general are very good, Fig. 10 shows that the prediction of the threshold for discriminating the pointing direction of an arrow is worse at small angular sizes of the arrow than at larger ones. A possible explanation is that there was more variation in experimental threshold values at the smaller angular sizes. Participants had difficulties in really seeing the actual direction of the road marking arrow at larger distances. Not surprisingly, we found the same effects of road surface

luminance and arrow size on the discrimination of the arrow direction, as could be expected from existing literature on the detectability of objects. Furthermore, in calculating the size of the road marking arrow we chose for the plane angle subtended by the length of the road marking arrow in front of the eye. Another option would have been to use the equivalent target size as reported in COST331 for transverse road markings which is expected to provide slightly larger angular sizes.

Having a contrast threshold value that varies with the road surface luminance and the size of the arrow is inconvenient when having to design road lighting concepts. Ideally, designers can make use of a single visibility threshold value, independent of the background and arrow luminance and the size of the latter. This single visibility threshold would allow road lighting designers to determine the minimal level and direction of illumination for detecting the direction of a road marking arrow. Not only the Probeam illumination concept would benefit from such a single visibility threshold; it would also be useful for the optimization of road lighting and car headlights in general. Hence, we evaluated multiple existing visibility measures to check whether they yielded a single contrast threshold value. In addition to Adrian's model, we applied image-based contrast models to an image cut out around the road marking arrow. We replaced the ΔL values by these contrast values to determine the corresponding visibility threshold of the contrast metric under consideration. Some of these measures resulted in more spread over the different background luminance values and some measures resulted in more spread over the different angular sizes of the arrow. Our results suggest that the Joulan et al. model allows for the largest reduction in the variation in contrast threshold across different angular sizes of the arrow, however, still with substantial variation (%) in contrast threshold across different road surface luminance values. Besides the Joulan et al. model, also the C_c , C_s , and C_{cs} contrast measures of the Tadmor and Tolhurst model show a reduction in variation (%) in contrast threshold across different angular sizes of the arrow and the road surface luminance values. Also, alternatively to the summation used in Equations 17 and 18, taking the maximum or average of all local (S)DoG was examined, however, we consider a summation more appropriate than

a maximum or average to account for the effect of size (i.e., the larger the arrow the larger the sum of DoG values; the smaller the arrow the smaller the sum of DoG values). The average CRAMM threshold values seem to indicate a bell-shape behavior as seen with the contrast sensitivity functions in Barten's research. Though, when considering the confidence intervals the bell shape of the curves might be an artifact. The large variation (%) and the relatively small C_{WLF} - values found with the Simone et al. model are most likely due to the fact that we used substantially lower luminance values as they recommended in their paper.

The Tadmor and Tolhurst, and Joulan et al. contrast models show promising results for achieving a unique threshold value, irrespective of background luminance, object luminance and object angular size for the experimental paradigm used in this study. These promising results suggest that image based contrast models allow to predict contrast thresholds in simulated road environments with a larger complexity, although more research is needed to improve the consistency, to optimize the parameters and to investigate the applicability of these models to the whole complex scene. Future research should also include more recent contrast models (Brémond 2020), and extend the analysis toward additional (natural) objects encountered while driving, as suggested in the study by Brémond et al. (2013). Furthermore, future work may include the replication of this study with more participants.

7. Conclusions

We measured luminance difference thresholds for a rendered highway environment consisting of a road marking arrow in positive contrast to a road surface. Luminance of the arrow and the road surface as well as the angular size of the arrow were considered as important parameters. Experimental data of the proportions correct detection of the arrow direction were used to fit a psychometric curve as a function of the difference in luminance between the arrow and the road surface for various experiment conditions. These fits were then used to determine the luminance difference thresholds, and the resulting values corresponded very well (R^2 of

0.75) with thresholds predicted by the Adrian visibility model, with the highest deviations occurring at the smaller angular sizes.

The results suggest that some image based contrast models allow for a reduction in the variation in contrast threshold across different angular sizes of the arrow and road surface luminance values. As such, these models show promising results, but didn't deliver yet the ultimate solution: a unique threshold value, irrespective of background luminance, luminance difference and object angular size.

Image based contrast models also allow to predict contrast thresholds in simulated road environments with a larger complexity, although more research is needed to improve the reliability and to optimize the parameters.

Acknowledgments

The authors would like to thank Willem Zandvliet and Duco Schreuder for their valuable feedback and comments.

Disclosure statement

No potential conflict of interest was reported by the author(s).

Funding

This research was financed and supported by the Directorate-General for Public Works and Water Management Rijkswaterstaat (The Netherlands). The first author was supported by the grant.

ORCID

Rik Marco Spieringhs  <http://orcid.org/0000-0003-4956-837X>

Kevin Smet  <http://orcid.org/0000-0003-3825-6274>

Peter Hanselaer  <http://orcid.org/0000-0002-6060-3706>

References

- Adrian W. 1969. Die Unterschiedsempfindlichkeit des Auges und die Möglichkeit ihrer Berechnung. *Lichttechnik*. 21 (1):2A–7A.
- Adrian W. 1989. Visibility of targets: model for calculation. *Light Res Technol*. 21(4):181–188.
- Aulhorn E. 1964. Über die Beziehung zwischen Lichtsinn und Sehschärfe. *Albrecht Von Graefes Arch Ophthalmol*. 167 (1):4–74.

- Barten PG. 1999. Contrast sensitivity of the human eye and its effects on image quality. Bellingham (WA): SPIE Press.
- Berek M. 1943. *Zeitschrift f. Instrumentenkunde*. 63:297.
- Blackwell HR. 1946. Contrast thresholds of the human eye. *JOSA*. 36(11):624–643.
- Blackwell HR. 1966. *Lighting handbook*. Vol 4. Illuminating Engineering Society, New York (NY). p. 2–8.
- Blackwell OM, Blackwell HR. 1980. Individual responses to lighting parameters for a population of 235 observers of varying ages. *J Illum Eng Soc*. 9(4):205–232.
- Brémond R. 2020. Visual performance models in road lighting: a historical perspective. *LEUKOS*. 17(3):212–241.
- Brémond R, Bodard V, Dumont E, Nouailles-Mayeur A. 2013. Target visibility level and detection distance on a driving simulator. *Light Res Technol*. 45(1):76–89.
- Cao Y. 2004. A Driving simulation based study on the effects of road marking luminance contrast on driving. *Transp Res Rec*. 1093:43–47.
- Clark RN. 1990. *Visual astronomy of the deep sky*. Cambridge: Cambridge University Press.
- Community BO. 2017. *Version Blender 2.79* [software]. Amsterdam (NL): Stichting Blender Foundation.
- COST. 1999. Requirements for horizontal road marking: final report of the action. Luxembourg: European Commission, DG Transport. Technical report COST 331 (Vol. 1). Luxembourg.
- Curcio CA, Sloan KR, Kalina RE, Hendrickson AE. 1990. Human photoreceptor topography. *J Comp Neurol*. 292(4):497–523.
- Donners MAH, Vissenberg MCJM, Geerdinck LM, Van Den Broek-Cools JHF, Buddemeijer-Lock A. 2015. A psychophysical model of discomfort glare in both outdoor and indoor applications. Proceedings of 28th CIE Session; 2015 June 28 – July 4; Manchester, UK. Vienna (AT): International Commission on Illumination. p. 216.
- European Committee for Standardization. 2015a. Road lighting part 2: performance requirements. Brussels (BE): CEN. Report No: CEN-EN 13201-2: 2015.
- European Committee for Standardization. 2015b. Road lighting part 3: calculation of performance. Brussels (BE): CEN. Report No: CEN-EN 13201-3: 2015.
- Fründ I, Haenel NV, Wichmann FA. 2011. Inference for psychometric functions in the presence of nonstationary behavior. *J Vis*. 11(6):16.
- Garcia PA, Huertas R, Melgosa M, Cui G. 2007. Measurement of the relationship between perceived and computed color differences. *JOSA A*. 24(7):1823–1829.
- Gescheider G. 1997. The classical psychophysical methods. In: *Psychophysics: the fundamentals*. 3rd ed. Mahwah (NJ): Lawrence Erlbaum Associates. p. 45–73.
- Hill J. 2002. Testing hypotheses about psychometric functions [Ph.D. thesis]. St. Hugh's College (UK): University of Oxford.
- Jakob W. 2010. Mitsuba physically based renderer. <https://www.mitsuba-renderer.org/>.
- Joulan K, Hautiere N, and Brémond R. 2011. Contrast sensitivity functions for road visibility estimation in digital images. Proceedings of 27th CIE Session. 2011 July 10–15; Sun City (ZA), Vienna (AT): International Commission on Illumination. p. 1144–1149. Sun City, South Africa.
- Kimura M, Hamada Y, Ikeda Y, Motomura H, Jinno M. 2019. Importance of a vector component and the vertical illuminance in road lighting for the obstacle visibility of the road. *J Sci Technol Light*. 42:17–21.
- Kruskal JB. 1964. Multidimensional scaling by optimizing goodness of fit to a nonmetric hypothesis. *Psychometrika*. 29:1–27.
- Kuss M, Jäkel F, Wichmann FA. 2005. Bayesian inference for psychometric functions. *J Vis*. 5(5):8.
- Mayeur A, Brémond R, Bastien JC. 2010. The effect of the driving activity on target detection as a function of the visibility level: implications for road lighting. *Transp Res Part F Traffic Psychol Behav*. 13(2):115–128.
- Ministerie van Infrastructuur en Waterstaat. 2019. *Richtlijn ontwerp autosnelwegen*.
- Ministerie van Verkeer en Waterstaat, Rijkswaterstaat. 1991. *Richtlijnen voor de bebakening en markering van wegen*.
- Mostafawy S, Kermani O, Lubatschowski H. 1997. Virtual eye: retinal image visualization of the human eye. *IEEE Comput Graph Appl*. 17(1):8–12.
- Rea MS, Ouellette MJ. 1991. Relative visual performance: a basis for application. *Light Res Technol*. 23(3):135–144.
- Rizzi A, Algeri T, Medeghini G, Marini D. 2004. A proposal for contrast measure in digital images. Proceedings of Conference on colour in graphics, imaging, and vision. 2004 Apr 5–8; Aachen (DE), Springfield (VA): Society for Imaging Science and Technology. p. 187–192.
- Sato M, and Hagio T. 2014. Visibility enhancement and power saving by pro-beam LED tunnel lighting method. *J Light Visual Environ*. 38:89–93.
- Scheir GH, Donners M, Geerdinck LM, Vissenberg MCJM, Hanselaer P, Ryckaert WR. 2018. A psychophysical model for visual discomfort based on receptive fields. *Light Res Technol*. 50(2):205–217.
- Schmidt-Claussen HJ. 1969. *Lichttechnik*. 21:126A (ref. Adrian 1989).
- Schütt HH, Harmeling S, Macke JH, Wichmann FA. 2016. Painfree and accurate Bayesian estimation of psychometric functions for (potentially) overdispersed data. *Vision Res*. 122:105–123.
- Simone G, Pedersen M, Hardeberg JY. 2012. Measuring perceptual contrast in digital images. *J Vis Commun Image Represent*. 23(3):491–506.
- Tadmor Y, Tolhurst DJ. 2000. Calculating the contrasts that retinal ganglion cells and LGN neurones encounter in natural scenes. *Vision Res*. 40(22):3145–3157.
- Wichmann FA, Hill NJ. 2001a. The psychometric function: I. Fitting, sampling, and goodness of fit. *Percept Psychophys*. 63(8):1293–1313.
- Wichmann FA, Hill NJ. 2001b. The psychometric function: II. Bootstrap-based confidence intervals and sampling. *Percept Psychophys*. 63(8):1314–1329.
- Wu J, Zheng C, Hu X, Xu F. 2011. Realistic simulation of peripheral vision using an aspherical eye model. *Retina*. 5:24.